EUROFUSION WPJET1-PR(16) 14900

S Wiesen et al.

Plasma-edge and plasma-wall interaction modelling: lessons learned from metallic devices

Preprint of Paper to be submitted for publication in
22nd International Conference on Plasma Surface Interactions
in Controlled Fusion Devices (22nd PSI)

This work has been carried out within the framework of the EUROfusion Consortium and has received funding from the Euratom research and training programme 2014-2018 under grant agreement No 633053. The views and opinions expressed herein do not necessarily reflect those of the European Commission.

Plasma-edge and plasma-wall interaction modelling: lessons learned from metallic devices

S.Wiesen[a], M. Groth[b], M. Wischmeier[c], S. Brezinsek[a], A. Jarvinen[f], F. Reimold[a], L. Aho-Mantila[b], JET contributors[d,*], The EUROfusion MST1 team[†], The ASDEX Upgrade team[c] and The Alcator C-mod team[e]

[a]Forschungszentrum Jülich GmbH, Institut für Energie- und Klimaforschung – Plasmaphysik, 52425 Jülich, Germany

[b]Aalto University, Espoo, Finland.

[c]Max-Planck-Institut für Plasmaphysik, 85748 Garching bei München, Germany

[d]EUROfusion Consortium, JET, Culham Science Centre, Abingdon, OX14 3DB, UK

[e]Plasma Science and Fusion Centre, MIT, Cambridge, MA 02139, USA

[f]Lawrence Livermore National Laboratory, Livermore, CA 94550, USA

Abstract

Robust power exhaust schemes employing impurity seeding are needed for target operational scenarios in present day tokamak devices with metallic plasma-facing components (PFCs). For an electricity-producing fusion power plant at power density $P_{sep}/R > 15$ MW/m divertor detachment is requirement for heat load mitigation. 2D plasma-edge transport codes like the SOLPS code as well as plasma-wall interaction (PWI) codes are key to disentangle relevant physics processes in power and particle exhaust. With increased quantitative credibility in such codes more realistic and physically sound predictions of the life-time expectations and performance of metallic PFCs can be accomplished for divertor conditions relevant for ITER and DEMO. An overview is given on the recent progress on plasma edge and PWI modelling activities for (carbon-free) metallic devices, that include results from JET with the ITER-like wall, ASDEX Upgrade and Alcator C-mod. It is concluded that metallic devices offer an opportunity to progress the understanding of underlying plasma physics processes in the edge. With the absence of carbon as the primary plasma impurity and given the fact that the edge plasma itself is hardly impacted by intrinsic metallic impurities it is possible to isolate the crucial processes relevant for plasma exhaust. The validation of models can be substantially

[*] See the Appendix of F. Romanelli et al., Proceedings of the 25th IAEA Fusion Energy Conference 2014, Saint Petersburg, Russia

[†] See http://www.euro-fusionscipub.org/mst1

improved by eliminating carbon from the numerical system. It is recognized that tokamak operations with metallic PFCs are more sensitive to PWI as the influx of sputtered high-Z material into the confined region must be kept low. Also, plasma fuelling can be impacted by prominent dynamic recycling effects. As a consequence edge and PWI models have been revised and furtherly developed to reflect the link between the main and edge plasma and the interaction with the wall components.
PACS: 52.30.Ex, 52.40.Hf, 52.55.Fa, 52.55.Rk, 52.25.-b

1 Introduction

Tokamak devices with metallic plasma-facing components (PFCs) have demonstrated to perform successfully preserving the first wall [1]. It has been shown that long-term fuel retention can be minimised [2] and metallic PFCs do allow for fast isotope exchange [3]. However, armour materials like tungsten or W-coated CFC have significantly lower heat load limits restricted by melting, embrittlement and recrystallization effects compared to graphite/CFC PFCs. Also, W-sputtering and an unfavourable neoclassical transport of W-impurities can lead to possible W accumulation which requires adequate accumulation avoidance techniques. As a consequence robust power exhaust schemes are needed for target operational scenarios in present day metallic devices. Due to the lack of the intrinsic carbon radiator baseline scenario discharges with improved confinement (e.g. H-mode) at high power require reliable exhaust schemes employing low-Z (Ne, N) or medium-Z (Ar, Kr, Xe) impurity seeding. For an electricity-producing fusion power plant at power density $P_{sep}/R > 15$ MW/m divertor detachment ($T_{e,plate} < 5$eV) is an additional requirement for heat load mitigation [4]. To meet such constraints in ITER or DEMO, a significant fraction of the power P_{SOL} arriving in the edge must be radiated away, and a radiation fraction $f_{rad} = P_{rad}/P_{SOL}$ of about 60% in ITER and exceeding 95% in DEMO (assuming 70% core radiation) is aimed for.

As no simple scaling for the particle and power exhaust problem exists, computational tools like the SOLPS edge plasma code [5] (or similar 2D or 3D edge codes) and plasma-wall interaction (PWI) codes are key for realistic and physically sound predictions of the life-time expectations and performance of metallic PFCs relevant for ITER and DEMO. This can only be accomplished when the numerical model is physically sound, complete and the relevant physics processes have been identified, disentangled and understood. Challenging the

employed numerical models against existing experiments is central for the validation process and important to increase quantitative credibility in the codes.

The carbon content in metallic device like JET has been massively reduced either by using He-discharges in JET-C (factor 7) or the use of D in the ILW (factor 10-20) which was related to an effective disabling of the carbon erosion process [6,7] (c.f figure 1). As a consequence of the reduction of the C-content it has been reported that in case of a carbon device like JET-C some of the relevant physics in the edge/SOL and plasma-wall interaction was masked by the impact of C on the plasma [7]. Thus, metallic devices offer an opportunity to progress the understanding of underlying plasma physics processes in the edge. Edge plasma and PWI modelling attempts suffered substantially from unknowns in the behaviour of the amorphous carbon PFC surfaces making a quantitative analysis of carbon transport and migration as well as the impact on the main plasma difficult. With the absence of carbon as the primary plasma impurity and radiator, and given the fact that the edge plasma itself is hardly impacted by intrinsic metallic impurities, it is possible to eliminate the free parameters for carbon transport from the models. Hence, with the metallic devices it seems to be simpler to disentangle the crucial processes relevant for particle and power exhaust from the impact of carbon transport physics otherwise observed in devices with C ad PFC [4].

It is noted however that tokamak operations with metallic PFCs are more susceptible to PWI as the influx of sputtered high-Z material into the confined region must be kept low [1]. Metallic surfaces do melt if they receive excessive heat loads and melt splashes can create dust particles which may lead to an increased level of tritium retention in ITER. Over the recent years it has become evident that the demand in reliable predictions of PWI employing material transport as well as melt and dust codes has actually risen since the establishment of metallic PFCs. In metallic tokamak devices plasma core fuelling and particle confinement is impacted as the prominent dynamic wall recycling effect has changed its nature with metallic PFCs [8]. Co-deposits can retain fuel effectively and subsequently release fuel into the main plasma by re-erosion of material. With the lack of carbon and with metallic PFCs such a ubiquitious fuel particle surface source does not exist anymore (apart from regions at which fuel can be stored in net-deposition zones for beryllium in JET-ILW) and particle retention and particle balance is influenced more by short time-scale dynamics [9]. New microscopic models to reflect fast retention and outgassing effects are required and currently being developed which in turn must be linked to improved recycling models to be used for edge plasma codes in the future. It is now well appreciated that modelling of metallic devices as

such requires generally more insight into the details of PWI physics. It follows that with the elimination of carbon from the numerical system the difficulty in tackling the power exhaust problem is not reduced but rather redefined due to the necessary inclusion of additional PWI physics.

The structure of this review is organized as follows: section 2 recapitulates used models for particle- and power physics and plasma detachment in carbon free environments. Section 3 discusses briefly the recovery of power fall-off lengths using edge codes, i.e. the basic features required for reliable edge numerical models. Sections 4 and 5 are central to this paper as they describe the recent activities in modelling power dissipation with radiation and the important issue of neutral transport and compression modelling. The ingredients of a robust edge model describing the full cycle of the transition into divertor detachment in L- and H-mode are discussed and summarized here. In section 6 the approaches to bridge between plasma edge physics and PWI are discussed which allow an integration of physics processes relevant for material migration and transport. In section 7 the need for global models integrating core/edge/PWI physics are highlighted focussing on the impact on pedestal physics. Section 8 concludes the paper.

2 Modelling power exhaust and divertor detachment in a carbon free environment

In a synthetic description of the power exhaust problem the energy dissipation in the plasma edge can be described as a step-ladder process [10]. Power from the confined region enters the plasma edge by anomalous (ballooning-like) cross-field transport and is mainly conducted along temperature gradients within the scrape-off-layer (SOL). Energy is transported along the magnetic field lines in the SOL downstream towards the divertor until it reaches an impurity radiation zone at which the temperature T is reduced and thus the heat-flux. As T is decreasing and after passing the ionization front at $T_e \sim 5$eV pressure is removed from the plasma by friction processes occurring between the plasma and the compressed divertor neutrals and a further reduction in T is the consequence. Additionally, plasma particles are lost by anomalous transport as well as charge-exchange (CX) processes, the latter leading to a spreading of energy by fast neutral particles. In the case that sufficient power could be dissipated or radiated away before reaching the target plate T can be further reduced to 2-3eV or below by strong volume recombination processes which cause a further loss of plasma particles. A transition into the detached regime is characterized by a roll-over of the plate

saturation current j_{sat} which will effectively reduce the target heat load even further as fewer particles recombine at the target plate surfaces (i.e. a smaller number of particles deposit their recombination energy of 13.6eV+4.5eV when D^+ is converted to D_2 at the wall). Additional particle loss like enhanced perpendicular transport or energy loss by other atomic processes like molecular assisted reactions, are acting as catalyzers in the increase of the degree of detachment [11-13].

For the highly non-linear process of power dissipation by divertor detachment no general scaling is available ([4] and references therein) which makes the application of at least two-dimensional predictive edge codes necessary like SOLPS-ITER [14], EDGE2D-EIRENE [15-17], SOLEDGE2D-EIRENE [18], SONIC [19-20], UEDGE [21]. Also interpretative codes like OSM-EIRENE [22] exist for which experimental plasma profiles are taken as model constraint input to derive for example transport coefficients. All such computational fluid (CFD) codes have in common that the Bragisnkii equations are solved for electron and ion energy, parallel ion momentum and particle balances for all species on a 2D non-orthogonal rectangular grid. Usually, a discrimination is done between the parallel (to the field) and the radial (perpendicular to the field) motion of the plasma as the nature of transport is different along the two directions (classical parallel vs anomalous radial). At all grid edges boundary conditions must be provided (e.g. Bohm sheath conditions at the target plates) in order to find a unique solution of the full CFD equation system. Common to all aforementioned edge codes is an iterative (sometimes time-dependent) coupling to the Monte-Carlo neutral kinetics codes like EIRENE [16], DEGAS [23] or NEUT2D [24] which solve the kinetic transport equations of Boltzmann-type providing the plasma source and loss terms within the volume and the interaction at the numerical system boundaries, i.e. the walls. As neutral particles are not bound to the magnetic field a 3D toroidal approximation of the neutral simulation grid is usually applied. The mean-free path of the neutrals can be large at low T_e (i.e. the Knudsen number $Kn >> 1$ in detached conditions) and thus geometric details become relevant to identify for example the neutral pressure in the divertor. A kinetic approach for the neutral transport is thus indispensable which allows also the inclusion of relevant atomic and molecular physics processes details.

In order to assess the power exhaust problem predictively for ITER and DEMO the codes must be validated against real experimental data. Unknowns in the model setup however hamper the validation process. For example an anomalous transport parameter for the perpendicular direction must be prescribed in an ad-hoc way. Transport in parallel

direction in case of strong gradients is not ideally described by a fluid approach and kinetic corrections (so called flux limiting factors) for heat and viscous flux have been implemented. Other model parameters to describe the boundary condition towards walls normally have to be prescribed, too (e.g. decay parameters for density and temperature), unless a model exists which describes the plasma up to the wall e.g. by grid extensions [18] and inclusion of a model for the sheath for glancing field line angles [25]. The list of *known* model parameters for which plausible predictions or robust scalings exist is not extensive and, to improve the model's credibility, the modeler usually seeks guidance from the experiment to identify those parameters for which no first-principles model exists.

With the possibility to eliminate carbon from the model the modeler is enabled to remove one large unknown: the amount of amorphous carbon eroded from the walls and the migration of carbon material to remote places, i.e. the localization of the carbon particle source, parametrized by inhomogeneous chemical erosion/deposition parameters. As a consequence this allows to ignore carbon transport and carbon induced radiation in general. Historically, it has been shown that the impact of carbon can be minimized by essentially switching off the chemical erosion process in helium plasmas. In the assessment of detachment in JET-C He-plasmas it has been shown [26] that the density limit seen in case of He is increased compared to D which occurs even after the formation of an X-point MARFE. Power detachment in He-plasmas occurs at a lower density than particle detachment, an effect which has been reproduced by SOLPS simulations, e.g. [27]. In such modelling investigations the quantification of C-source could be neglected and the relevant processes could be easier identified which led to the actual understanding of the experimental observations (here for He-plasmas: a reduction of the ionization rate leads to longer mean-free paths and together with lower rates for CX and elastic collisions the He penetration is increased, hence a higher density could be achieved before a pressure collapse induced by dominant HeII radiation.). The consequence of a missing efficient intrinsic radiator is that another impurity radiating species is required to allow further power flux reduction towards the PFCs and the extrinsic impurity's transport characteristics must be assessed.

It should be noted that 3D edge plasma models do also exist which can be employed for the case when the 2D picture above of power and particle exhaust breaks. Fluid-kinetic 3D models like the EMC3-EIRENE code [28-30] are specifically needed if resonant magnetic perturbation coils (RMPs) are in place as it is planned for example for ITER. However, such codes like EMC3-EIRENE have their own limitations on top compared to the 2D codes and

the validation process of the 3D codes has only begun as their development progresses at the same time. Nevertheless, all following conclusions about model improvements in absence of carbon using 2D codes are generally valid also for 3D codes.

3 Recovery of power fall-off length and dissipation scalings

One critical constraint for any edge plasma modelling attempt is knowledge about the upstream conditions, i.e. information about plasma profiles close to the separatrix at the midplane. From multi-machine regression analysis [31-32] a robust scaling expression has been derived for the power fall-off parameter λ_q representing the power flux density $q_{||}^{max} \sim P/R\lambda_q$ close to the separatrix at the outer-midplane location. No size dependence on the major radius R was found but an inverse proportionality with the poloidal magnetic field strength B_p (or I_p). Scalings for λ_q have been derived from L- and H-mode discharges for low-density (attached) conditions assuming negligible volumetric power losses. A high level of regression confidence could be gained by covering JET, AUG, MAST, C-mod, DIII-D and from this it has been followed that the same scalings hold for both carbon and metallic devices.

A leading theory to explain the simple λ_q-scaling is the so called heuristic drift model (HD model) proposed in [33] which suggests that the width power flux tube is essentially a result of balancing Pfirsch-Schlueter (PS) flows against particles losses from the plasma core driven by vertical magnetic drifts (grad-p and curvature drift) and parallel losses along the field towards the divertor plates. As a consequence the PS return flows are of the order half sound-speed and large up-down ion pressure asymmetries are required. Consistent with experiments and within the simple flow picture one can estimate a minimum density width $\lambda_n \approx 2(a/R)\,\rho_p$ with ρ_p being the poloidal ion gyro radius. The model furthermore assumes that the region with width λ_n is filled with energy by anomalous electron thermal conduction from the core which is balanced by parallel Spitzer thermal conduction. From this one concludes then that $\lambda_q^{HD} \approx \lambda_n$. The HD model fits excellently into the scaling database from [31]. In standard edge plasma codes like SOLPS no such physics based anomalous transport model exists. Instead average values for the diffusive transport parameters $D_\perp$ and $\chi_\perp$ or pinch-velocities $V_\perp$ have to be adjusted to mimic the radial anomalous transport within the SOL. With the λ_q -scaling at hand a modeler can restrict the upstream transport parameters to a plausible level even without having a first principles model implemented. An important feature of the HD model is the fact that it does not require an adhoc anomalous particle diffusivity as it is based on drift flow and SOL current physics. Recent attempts to recover the

λ_q^{HD} scaling by using the SOLPS-ITER code including fluid drifts and electric potential relaxation in the model have shown to be very promising as almost no dependence on the value of $D_\perp$ was derived for λ_q when magnetic and ExB drift worked together [34].

Target heat flux profiles q(s) along the target are usually measured by means of infrared thermography and/or Langmuir probes [35] and a unique parametrization exists which consists of a convolution of an exponential decay (with decay parameter λ_q) with a Gaussian function representing the spreading of heat in the divertor, SOL and private-flux region (PFR) [31]. The integral power decay length [36] is defined ad $\lambda_{int} = \int(q(s)-q_{BG})ds / q_{max}$ which is well approximated by the simplified expression $\lambda_{int} \approx \lambda_q + 1.64\ S$ [37]. S is the so called power spreading parameter. Recently, a complementary database of the parameter S has been collected and analyzed from AUG and JET outer target IR measurements for L-mode and H-mode discharges [38]. A regression analysis for the H-mode data revealed a scaling mainly driven by the size of the machine (major radius) R_0 and the poloidal magnetic field B_{pol}, i.e. $S_{Hmode} \sim R_0/B_{pol}$ with a slight power dependence but no density dependence. The regression of the L-mode data revealed no size dependence but a clear linear dependence on density, i.e. $S_{Lmode} \sim n_e/B_{pol}$. These S parameter scalings include data from AUG and JET with carbon wall, as well as for AUG with the full-W wall, varying also the divertor configurations (horizontal and vertical target). Accompanying modelling using SOLPS [38] has reproduced similar S parameter scalings for both, L- and H-mode, and for each of the divertor configurations separately. The modelling supports the experimentally observed fact that there is no deviation from the scalings if carbon is removed from the system (i.e. in the model by switching off C sputtering and replacing the missing C radiation by D radiation with increased gas-flux). The model reproduces the increase of S by a factor of 2 in case of vertical target configurations compared to horizontal configuration, a result which is related to higher n_e and lower T_e in the divertor due to localized radiation patterns closer to the targets. The model has eventually predicted a robust reciprocal dependence on the target electron temperature $T_{e,targ}$ as the best ordering parameter for the S-scaling, i.e. $S \sim 1/T_{e,targ}$, for all simulation cases, a dependence which was derived with a high level of confidence. The SOLPS simulations clearly indicate that the S parameter is mainly given by the density profile width at the target which depends on the T_e-drop along the field lines near the separatrix. This drop is either induced by radiation, 2D nature of heat transport (radially anomalous vs parallel conductive) or interaction with neutrals. As observed in the experiments, for the same $T_{e,targ}$, the SOLPS model gives the same S (but not necessarily the same λ_{int} as λ_q may vary). It is important to

note that the numerical scaling has been derived assuming no change in the transport assumptions for perpendicular transport. It remains open in what way the expression for S is influenced by varying anomalous transport effects.

The fact that a simple dependence for $S(T_{e,targ})$ could be derived for all the analyzed data (JET and AUG, H- and L-mode, with and without C as well as varying divertor configuration) reflects the fact that an increase in S is a pure consequence of the way how T_e is reduced along the field in the SOL and hence, the scaling for the power spreading parameter S depends only indirectly on the wall material. The relevant mechanisms leading to significant power dissipation in the plasma edge and in the divertor are manifold (impact of system size, divertor geometry, neutral compression, radiation loss, 2D nature of transport) and edge codes reflecting those details must be validated and benchmarks against each other for reliable predictions.

4 Modelling power dissipation with radiation

From the λ_q-scaling the upstream parallel power flux density $q_{||}$ in ITER will be approximately 5 GW/m^2 and in the demonstration power plant DEMO $q_{||}$ will exceed 30 GW/m^2. The unmitigated perpendicular power flux density at the target plates is estimated to be 50 MW/m^2 and 300 MW/m^2, respectively [4], which would clearly exceed the tolerable material limit of 5-10 MW/m^2 (using W as actively cooled armour PFC material). Reliable power dissipation mechanisms like radiation losses or exploitation of charge-exchange processes or transport of plasma to distribute the power loads onto the walls are required to dissipate a major fraction of the total loss power entering the edge from the core. In metallic devices the lack of carbon has the consequences that the missing intrinsic radiator must be replaced by an externally applied impurity seeding species in order to starve the power flow into the divertor allowing heat load mitigation and also control of high-Z material sputtering. With intrinsic C missing also in ITER and DEMO externally puffed impurities (like Ne, Ar or Kr) are essential to impose a strongly radiating regime and to allow for significant radiation losses, i.e. radiative fractions $f_{rad} = P_{SOL\text{-}edge}/P_{rad}$, of about 60% in ITER and exceeding 95% in DEMO (assuming that up to 70% can be radiated in the confined region).

In existing metallic devices stable radiative discharges at large f_{rad} have been established. In JET-ILW a radiative fraction f_{rad} =70-75% at a maximum power density

$P_{heat}/R \sim 9$ could be achieved with nitrogen seeding [39]. Complete divertor detachment at both targets has been observed concomitantly with strong X-point radiation. Similarly, AUG reaches a radiative fraction up to $f_{rad} \sim 80\text{-}85\%$, a larger value compared to JET which is partly related to the larger W concentration in AUG due to the W main chamber wall. Both devices happen to operate also in a pronounced detachment regime in case of strong X-point radiation. A record power density of about $P_{heat}/R \sim 14$ was achieved in AUG [40]. ITER or DEMO will require $P_{heat}/R \sim 20$ or higher. In order to predict the dissipation performance of a next step fusion device the existing modelling tools need to proof that they can reproduce the full transient leading into detachment.

Nitrogen and Neon seeded JET H-mode discharges [41] have been analysed with EDGE2D-EIRENE [42] and reproduced qualitatively well the transition form an attached regime into partial detachment induced by impurity radiation. With the increase in the radiative power P_{rad} a 5-10 times reduction in the peak target heat load at the LFS $q_{peak,LFS}$ has been obtained with both, Ne or N seeding. Compared to the experiment the radiation loss is underestimated within a factor 2. In these JET plasmas a radiated fraction frad ~50-55% has been reached. The code predicts also numerically stable pronounced detachment regimes at a higher level of f_{rad}, i.e. towards similar values observed at JET achieving a maximum $f_{rad} \sim$ 70-75% with complete LFS detachment [4]. The code does also predict the radiation patterns. Neon is predicted to be a factor 5-10 stronger mantle radiator and radiates in the SOL as well as close to the pedestal. Nitrogen on the other hand radiates mainly in the divertor. Non-coronal effects [43-44] are automatically included in the edge simulations and impurity transport effects lead to an enhancement of radiation by broadening of radiative power function $L_z(Te)$ for a given impurity species (c.f. fig. 2). Therefore N radiates in a broader temperature range 10-30 eV and Ne 20-150eV explaining the large difference in the radiation patterns observed.

A detailed analysis of the H-mode detachment transition has been pursued for AUG N-seeded discharges [45-46]. First with increasing density (and with no seeding) the onset of detachment is observed a the HFS divertor. As the density increases further a fluctuating regime is observed with fluctuations at the X-point. Additionally, the establishment of a HFS high-density (HFSHD) region is observed [47] which can be sustained by a significant fraction of power carried in the HFS far-SOL towards the divertor plates. With external seeding (e.g. N) LFS divertor partial detachment is triggered concomitantly occurring with strong N-radiation close to the X-point. At the same the HFSHD region disappears. With

increasing the N-seeding even further a complete detachment regime can be established in which radiation (nitrogen and Balmer) is mainly condensed inside the confined plasma, i.e. at the X-point (c.f. fig. 3). The propagation of the radiation front towards the X-point is in parallel with a temperature loss just inside the confined region above the X-point. The strong X-point radiation triggers a loss in the pedestal pressure, i.e. a depletion of $T_{e,ped}$ and $n_{e,ped}$ driven by transport along poloidal gradients into the X-point regions. Similar observations of pedestal pressure loss with impurity have also been observed in JET [39].

SOLPS modelling is able to reproduce the full transition from attached to complete detachment in seeded H-mode. The standard procedure is to fix for a given level of density the upstream and downstream diffusive transport to values which allows to match plasma profiles measured by Li-beam, Thomson-scattering and CXRS measurements (upstream) and at the same time target profiles measured by Langmuir probes and IR tomography. The full path of particles and radiation disconnecting from the targets in a partial detached regime until complete detachment with condensation of density and radiation close to the X-point can be reproduced with the code [48]. An essential ingredient is the inclusion of cross-field drifts to ensure in/out asymmetries. Although the transition into detachment can be understood some caveats still exist in this approach as some quantities could not be matched. For example in the complete detached state the fueling and seeding rates assumed in the model are to low compared to the experiment (factor 5-8) and consequently the neutral pressure is too low, too (factor 2-6). In order to match the downstream profiles an increase of radial transport in the divertor was necessary (factor 3) and additionally a separate rescaling for the HFS/LFS transport was necessary. With this caveat, still, SOLPS is able to recover also the upstream pressure loss mechanism for both, showing a stronger impact on the depleation of $T_{e,ped}$ with Ne-seeding compared to N-seeding (explainable by different radiation patterns and thus impact of the radiation loss function $L_z(Te)$)

With this result it seems that one must accept that the validation of a code like SOLPS is hampered as for each level of density a separate scaling of the transport is necessary to match up- and downstream profiles. The trend to increase the transport at higher density has led to parameterisations of anomalous transport for example by scaling it with plasma parameters like collisionality or density [49]. This rescaling method using feedback on the plasma solution helped in terms of allowing a particle flux roll-over at lower density (i.e. closer to the experimentally observed value) but did also lead to numerical oscillations in the completely detached case making again a validation hard.

It has only been recently reported [47] that a tremendous improvement could be achieved in terms of transport prescription making a rescaling procedure unnecessary. By assuming an extra advective transport loss channel for anomalous transport in the SOL and at the same time reducing the pedestal transport it is possible to reproduce the full-cycle of detachment transition including the establishment of the HFSHD region without rescaling of diffusive transport. Still, a model for cross-field drifts needs to be included to reproduce the in/out asymmetries but the deficiency to underestimate the required fueling and seeding rates as well as a too low divertor pressure has been effectively eliminated by this method. As no feedback of the plasma on the transport parameters is assumed in the model numerically stable solutions for each density of the detachment transition cycle should be achieved. If this method proves to be successful in future, this could then be regarded as a significant step forward for the validation of edge codes for power exhaust.

5 Neutral transport and divertor compression and impact on power exhaust modelling

In metallic devices the way the plasma is recycled at the PFCs has changed significantly. With no C present on the recycling surface the particle source by chemical erosion has been effectively switched off causing the particle content essentially to be defined by the total particle throughput Φ. Metal PFCs are also able to sustain specific kinetic transport effects, e.g. competitions between slow moving particles being reemitted from the surface as recycling neutrals and fast ballistic neutrals from charge-exchange processes or surface reflections (c.f. fig. 4). This can have consequences on the core plasma fueling as it was shown in EDGE2D-EIRENE simulations for seeded JET H-mode discharges [50]. In these simulations the radiation fraction has been increased by N-seeding and the influx of fuel particles had been compared between (semi-) horizontal (HT) and vertical target (VT) configurations. At large radiative fractions f_{rad} the influx of D atoms from LFS in HT is a factor 6 stronger than in VT, whereas at lower f_{rad} both VT and HT behave similar in terms of core fueling. This effect cannot be related only to the pedestal pressure loss at high f_{rad} as pressure loss occurs in both VT and HT configurations in similar ways. Rather the drastic change of the LFS fueling in HT must be related to the qualitative change of neutral transport, i.e. ballistic effects of fast neutral particles fueling more efficiently the LFS in HT.

In metal devices the divertor configuration itself and neutral kinetics have a stronger impact the neutral distribution in the volume and thus the level of neutral compression in the

divertor. It is thus important to model a seemingly more delocalized neutral distribution correctly and to validate this neutral model for example against pressure gauge measurements. The difficulty in modelling neutral compression has been highlighted the model-based radiation scalings which had been derived for N-seeded JET-ILW and AUG discharges in L-mode using the SOLPS5.0 code [51]. The model was quite successful in identifying three radiative regimes which are in line with the experimentally observed data: 1) a low radiating regime (f_{rad} ~ 5-10%) with most of the radiation located in the inner divertor, 2) a regime with maximum level of radiation in the divertor up to f_{rad} ~ 60%, and 3) maximum total radiation with the radiation front moving above the X-point i.e. into the confined region. The model does also reproduce well the experimentally observed radiative asymmetry in the divertor legs if cross-field drifts (ExB and grad-B) are included. But there had been drawbacks as well. On the one hand the model recovers qualitatively well the empirical scaling law for divertor radiation with increasing N2 injection taken from [52], i.e. $P_{rad,div} \sim p_{0,div}^{0.5} R_0 \lambda_q (Z_{eff}-1)^{0.3}$ with $p_{0,div}$ the neutral pressure in the divertor, on the other hand the scaling underestimates the modelled JET-ILW data by a factor 0.4 whilst the match with AUG is better and within a factor 1.2. This discrepancy can be partly related to the fact that, contrary to AUG, the modelled JET discharges were in semi-horizontal divertor configurations with the LFS strike-point located on the horizontal target and thus stronger pump action of neutral impurities into the LFS corner pump throat is expected, the latter however was not correctly included in the SOLPS model. Hence the main model uncertainty is in fact related to the difficulty to estimate numerically $p_{0,div}$ with the code. And this is specifically difficult for JET case as, contrary to AUG, a good coverage with pressure gauges is lacking which otherwise would allow a better validation of the kinetic neutral transport model EIRENE being part of the SOLPS package.

The impact of the neutral distribution on detachment has been analyzed in greater detail for JET-ILW unseeded L-mode discharges for (semi-) horizontal (HT) and vertical target (VT) configurations using the EDGE2D-EIRENE code package [53]. Here the transport in EDGE2D was purely diffusive and fixed for all densities but cross-field drift were included. The result was that with increasing LFS upstream density $n_{e,sep}$ the predicted roll-over of the LFS and HFS plate-integrated ion currents $I_{div,HFS}$ and $I_{div,LFS}$, respectively, occurs close to the same $n_{e,sep}$, slightly shifted to 10-15% lower $n_{e,sep}$ in VT than in HT configuration. This is consistent with the experimental data. However the behavior of the predicted LFS peak plate temperature $T_{e,pk,LFS}$ is not: $T_{e,pk,LFS}$ drops down below 2eV at 30% lower $n_{e,sep}$ in VT than in HT configuration, a prediction not seen in the experiment. This discrepancy could

not be fixed by switching on cross-field drifts in EDGE2D-EIRENE as this was resulting in dropping the HFS $T_{e,pk,HFS}$ only but kept $T_{e,pk,LFS}$ similarly low as in the case without drifts. A model to mimic a by-pass leak at the tile gap of the LFS vertical target plate also did not raise $T_{e,pk,LFS}$ either as the neutral density in front of the tile gap is too small to impact the overall recycling at the LFS plate. In [53] a deeper analysis of the neutral fluxes towards the pump throats revealed that 80% of the total injected deuterium has been pumped at the LFS in HT whereas in VT it was only 30% (assuming equal pumping speeds or albedos at the pumping corner surfaces). This was unexpected as with consideration of the neutral conductance and shorter path lengths of the neutrals reaching the cryopump in JET at the LFS, the LFS pump should be more efficient. Indeed the simulations indicate that neutrals which have to travel through the PFR to reach the LFS pump to could compete well with the reflected ballistic neutrals from the metallic plates in HT into the LFS pump throat. However it was evident that the total amount of neutral pumping (i.e. the particle throughput) Φ_D was approximately a factor 3 lower compared to the experiment to reach the detachment roll-over. As an additional difficulty the neutral divertor pressure $p_{0,div}$ could not be benchmarked as the only available pressure gauge in JET is located 2m below the divertor baseplate, in the lower part of the so-called sub-divertor region.

A subsequent improvement of the neutral model in EDGE2D-EIRENE includes an extension of the neutral EIRENE simulation grid into the sub-divertor region [54] that was capable to include the neutral conductance towards the cryopump, leakages around the divertor as well as the location of the sub-divertor pressure gauge. The same discharges as in [53] have been analyzed again and a clear linear relationship between the throughput Φ_D and the measured $p_{0,sub-div}$ was found, i.e. $\Phi_D/p_{0,sub-div}$ = const, that agrees well with the experiment. The required experimental value of Φ_D was a factor 2-3 higher in VT than in HT to reach a given upstream density $n_{e,sep}$, a result reproduced by the extended EDGE2D-EIRENE model including the sub-divertor model within a factor of 2. At lower $n_{e,sep}$ the pumping is more balanced in VT compared to HT, albeit this is not the cause for a higher Φ_D required in VT. It is rather the number of neutral particles capable to penetrate the separatrix which being smaller in case of VT requiring a larger Φ_D to reach a given $n_{e,sep}$, i.e. requiring a greater particle content. At higher $n_{e,sep}$ the situation is different: the neutral penetration across the separatrix is similar in HT and VT but the pumping is increased in VT due to particles reaching the cryopump either below the PFR plasma or circumventing the plasma by recirculation of neutrals leaving the LFS pump throat reaching the cryopump through the sub-

divertor structures (c.f. also the benchmark work using the DSMC code DIVGAS [55-56]). From the model linear dependencies for the neutral pressures at the LFS and HFS pump throat, $p_{0,div\text{-}LFS}$ and $p_{0,div\text{-}HFS}$ respectively, are derived as function of $p_{0,sub\text{-}div}$: in VT $p_{0,div\text{-}LFS} \approx p_{0,div\text{-}HFS} \approx 6p_{0,sub\text{-}div}$ and in HT $p_{0,div\text{-}LFS} \approx 6\ p_{0,sub\text{-}div}$ and $p_{0,div,HFS} \approx 4\ p0,sub\text{-}div$. These factors are only valid for the considered unseeded L-mode density scan. Reviewing the model-based scaling attempt from [51] described previously and with the assumption that $p_{0,sub\text{-}div}$ instead of $p_{0,div\text{-}LFS}$ has been assumed in the reproduction of the scaling of $P_{rad,div} \sim p_{0,div}^{0.5} R_0 \lambda_q (Z_{eff}-1)^{0.3}$ the missing factor 0.4 for JET-ILW in [51] is recovered by the mismatch between $p_{0,sub\text{-}div}$ and $p_{0,div\text{-}LFS}$, i.e. 1/sqrt(6).

A quantitative assessment of the dominant atomic and molecular processes governing the neutral dynamics has been discussed in [57] using the OSM-EIRENE interpretative model for Alcator C-mod. C-mod, having a small major radius of 0.65m, can be regarded as relevant for ITER in the sense that the average density is higher than in other devices and thus C-mod has "ITER-like" features (vertical divertor targets and large neutral pressures) which allows to validate the physics model relevant for ITER conditions. In order to match the neutral pressure and Balmer radiation profiles within a factor of 2 using OSM-EIRENE the following processes had to be included: Ly-α opacity, neutral viscosity, molecular assisted recombination (MAR) as well as ion-molecule elastic collisions. All these processes had been included in the ITER design studies [58, 11] and in principle all those processes can be included in all edge codes with coupling to EIRENE. Recently, it has been reported that a radiation short-fall was recovered in the modelling of unseeded JET [42, 53, 59] or AUG [48] discharges (with metallic walls) using SOLPS or EDGE2D-EIRENE. The short-fall is characterized by a factor of 2-10 lower D_α line emission compared to spectroscopic measurements and occurs even if the neutral divertor pressure is matched to the experiment and with or without N-seeding. At high densities this could be related to missing terms in the D_2 and D_2^+ molecule dissociation [59] following emissions of electronically excited D atoms. Such terms, if significant, should be accounted for in the calculation of the emitted D_α radiation in the model and/or in the corresponding energy sink terms passed over from EIRENE to the plasma fluid code. Some initial attempts to include losses from Fulcher atoms into EIRENE have not eliminated the question of D-radiation short-fall so far and it is still an unresolved issue. In the total power balance of for example high-power seeded discharges the D-radiation short-fall plays however only a minor role.

Recent predictive simulations for Alcator C-mod [60] using the new SOLPS-ITER code [14] including the Kotov-2008 model [11] support the fact that adding neutral leakage paths in the model is indeed essential for the correct modelling of divertor conditions, specifically for the case of high density. The C-mod plenum pressure is very sensitive to the level of geometric details included. The impact on the plasms solution itself is not sensitive to details of the actual leakage path however the sole existence of leakage paths has a strong impact on the neutral pressure and thus on the plasma solution (i.e. no leakage into the C-mod plenum leads to a too cold divertor plasma). With the inclusion of leakages and cross-field drifts at the same time an excellent agreement for the upstream profiles could be achieved (in both, forward and reversed field configurations). The LFS target profiles match also excellently with the Langmuir probe data and $T_{e,plate}$ asymmetries are reproduced. However, the transition into HFS detachment remains elusive. It is hoped that also this last discrepancy can be resolved by improving the transport model of the plasma, e.g. assuming an advective component for the anomalous transport as suggested in [47].

To conclude on this and the previous section it is summarized that for a reliable 2D power exhaust edge model all the following features should be included in order to reproduce the full cycle of the transition into detachment (with or without seeding)

- cross-field drifts (i.e. ExB and grad-B drifts)
- a complete as possible kinetic neutral physics model including volume recombination, charge-exchange, and at in dense divertor conditions neutral viscosity, elastic collisions as well as molecular assisted processes and Lyman opacity
- a representative geometric model for the vessel in 2D (and if necessary in 3D), including main-chamber, divertor and sub-divertor structure that can incorporate also neutral conductance through leakages and gaps behind the PFCs up to the pumping surfaces and available pressure gauges
- a SOL transport model which does reflect also the non-diffusive nature of anomalous transport
- an extension of simulation grid into the pedestal region in 2D to reflect the impact of X-point radiation (and radiative belts) on the pedestal pressure and transport

We furtherly note: the compression of fuel and impurities is assumed to be purely a function of the individual particle throughputs Φ_n and in steady conditions not influenced by the wall if not otherwise necessary (e.g. for N stickiness at the walls). Generally, the impact on particle content by wall erosion processes is assumed to be minimal. The impact of impurities on power dissipation through radiation can thus be assumed to be disconnected from the metallic wall conditions as metallic impurities themselves only have a small impact on the cooling of the SOL. In steady conditions assuming a constant level of power from the core (i.e. in L-mode and in inter-ELM H-mode phases) the actual composition of the wall material only plays a role for varying particle reflection coefficients when switching from W to Be or Mo. The ballistic processes of reflection and recycling of neutrals are already included in the kinetic EIRENE code.

6 Integrated PWI modelling

With increasing density particle losses in radial direction towards the main-chamber increase. When approaching divertor detachment the particle flux rolls over at the target plates and the global particle flow pattern must account for this by enhanced transport perpendicular to the field for plasma and neutral particles (only part of the global particle loss is accounted by volume recombination). Li-beam measurements at AUG and JET have shown that with the increase of the Greenwald fraction f_{GW} the radial density profile flattens [61]. Also a formation of density a shoulder has been observed with increase of density which can be linked with the actual divertor geometry of the discharge (depending to the closure of the divertor ballistic effects in neutral transport, c.f. [62]). The increase of perpendicular flux with density has been observed also in COMPASS [61], DIII-D and C-mod [63], TCV [64], KSTAR [65]. The increase of radial plasma transport with collisionality has also been recovered regularly by simulations ([64-67] and references therein) highlighting the role of interchange instability driven turbulence.

With the increase of flux towards the main-chamber walls effects from plasma-wall and neutral-wall interaction like material erosion becomes more relevant. Specifically, the assessment of Be erosion, migration and particle retention in Be co-deposited layers has become an important issue for ITER [7]. A detailed investigation to assess the amount of Be produced and transported to remote areas leading to co-depostion, fuel retention and also dust formation is required. An integrated approach is thus necessary for bringing together the first wall flux dependencies and the actual PWI processes involved. Historically, standard edge

tools like EDGE2D-EIRENE or SOLPS have not taken into account the direct interaction of the plasma with the main-chamber wall as the simulation grid was not in direct touch with the walls surfaces. Recent developments however in the code SOLEDGE2D-EIRENE has led to the implementation of a so called wide-grid extension of the simulation grid up towards the first wall [18]. Similar code extensions are currently also in preparation for the SOLPS-ITER code package. Without the extension of the grid usually the codes assume that the plasma decays with a fixed decay length at the grid boundary, somewhat closer to the separatrix. Only the EIRENE neutrals in any of the aforementioned codes could interact with the first wall and the exposure of PFCs to energetic CX neutrals were already discussed in the past. With no grid extension to the wall however the plasma particle fluxes measured with Langmuir probes could not be matched [68] and consequently the calculation of erosion fluxes and global impurity yield depended strongly on the assumed boundary conditions. Combined OSM-EIRENE/DIVIMP simulations with no grid extension predicted a variation of Be erosion fluxes within at least one order of magnitude [69]. Now with a grid extension included the flux towards the wall is a function of the overall plasma solution and the assumed anomalous transport model and the free decay length input parameter can be replaced by a proper sheath physics model at the wall. SOLEDGE2D-EIRENE has included an improved model for the plasma sheath boundary conditions for the case of glanzing angles [25]. First simulations for a JET-ILW L-mode discharges showed that additional erosion zones near the top-plane and at the LFS first wall could be recovered and thus led to the observation of a rather inhomogenous Be-erosion pattern [18].

Recently, the Be erosion process has been thoroughly assessed by molecular dynamics (MD) codes in greater detail. It was found that in addition to the physical sputtering process a chemically assisted sputtering channel producing BeD_x molecular compounds has been identified numerically [70] and also experimentally [71]. The BeD sputtering process requires a finite level for the projectile impact energy E_{D+} and increases with E_{D+}. Recent MD simulations have also shown that a dependence of the surface baseplate temperature T_{base} exists too, i.e. a decrease of the BeD yield with increasing T_{base} [72]. Also this has been recovered by spectroscopic gas-balance [71] resulting in the observation that with increasing T_{base} the amount of D produced by BeD erosion can be compensated with D from dissociating D_2. A new database including the full set of Be erosion processes has been derived from the MD simulations to be used in PWI codes like ERO. A comparison of the effective total Be erosion yield as a function of $T_e < 30$eV calculated by ERO [73] shows a fair agreement to the

measurements (with a factor 3-5). Above T_e=30eV the Be yield is strongly enhanced by Be self-sputtering.

To assess the particle fluxes and erosion patterns into remote areas in JET-C and JET-ILW a comparative study using the ERO Monte-Carlo code [73]. In this case the divertor plasma background parameters have been parametrized (radial density and temperature profile widths, impurity concentrations, etc) to allow a larger flexibility in the sensitivity studies pursued. The ERO simulations reproduced the experimental result that high-Z material influx by W-sputtering is only by ELMs in H-mode discharges and that a finite level of Be is transported into remote areas due to reflections at W-PFCs. Hence, for Be migration, kinetic effects play a major role. Transport of neutral Be particles seems to be responsible for fluxes into regions below the horizontal target, not accessible by the plasma. For both, JET-C and JET-ILW, the fluxes of intrinsic low-Z impurities into remote areas are qualitatively similar. A slightly stronger dependency on the divertor geometry (strike-point location either on VT or HT) is recovered in JET-ILW due to ballistic effects. In absolute numbers the deposition rate is a factor 10 smaller compared to the collector probe. New shot-resolved QMB experiments are under way to better quantify and validate the ERO model [73].

7 Towards global modelling

With emerging of sophisticated databases for the Be sputtering yields plus the possibility to derive the actual particle flux arriving at the first wall with grid extensions one is in a better position to understand the global Be material migration process, transport and particle retention at the same time. The combination of the WallDYN-DIVIMP code package [74-75] has the capability to achieve exactly this. WallDYN splits up the first wall (main-chamber and divertor) into a number of segments, each representing a PFC consisting of a near-surface reaction-zone and deeper lying bulk-zone. The information about particle fluxes (bulk plasma and/or impurities) is taken for example from a SOLEDGE-EIRENE simulation and is distributed across the set of PFC segments. The impurity Monte-Carlo code DIVIMP is then used to calculate the particle transport of the eroded particles from each segment to another. The yield coefficients for erosion and sputtering are taken from revised MD simulation databases. As a result one derives a migration matrix telling how much material has been transport from each source segment to another destination segment. With this approach it was for example possible to confirm the experimentally observed migration and deposition pattern of Be, i.e. a net deposition zone on top of the HFS upper baffle plate on top of the JET-ILW

divertor [76]. Another example is the transport of N using the WallDYN package [77]. The availability of a global migration code WallDYN-DIVIMP combined with validated extended plasma backgrounds from SOLEDGE2D-EIRENE or SOLPS-ITER is a major step forwards in the field of integrated modelling predictions for ITER and DEMO.

ERO simulations have shown [73] that W erosion between ELMs in H-mode discharges is small compared to the amount of erodded W at the ELM which can be significant. With no suitable W source control scheme a high-power H-mode discharge will suffer significant core plasma W accumulation. This is a control issue for power exhaust and core plasma performance at the same time (c.f. [78]) as W accumulation avoidance techniques like ELM-flushing or RF heating schemes interplay with other W source reduction schemes like power flow reduction towards the W PFCs by detachment. Integrated models bringing together core physics with edge/SOL physics are required to establish global models for scenario developments towards ITER and DEMO which need to be first benchmarked against high-power discharges in existing metal devices.

Integrated core/edge/SOL/PWI models (c.f. fig. 5) do already exist [79-82] and depending on the flavour the sub-models for core-, SOL/edge- or PWI-physics are superior or inferior to others. A bold example where integrated modelling is required is linked to pedestal physics and transport and the change thereof with change of PWI physics. It has been observed in JET-ILW that compared to JET-C the pedestal density evolution is retarded after an ELM-crash. A similar evidence for the change of the pedestal behavior has been found in AUG [83]. The duration it takes to build up the n_e- and T_e-pedestal after an ELM seems to be dependent on the level of recycling and varies between 1-10ms in JET-ILW [84] and pedestal height depends also on selected divertor configuration and pumping [85]. Time-dependent EDGE2D-EIRENE simulations of ELM dynamics on their own were not capable to explain the retarded pedestal refueling process [86] as these assumed a fixed model for the transport in the pedestal region. A hypothesis has been suggested that the pedestal fueling could be impacted by dynamic outgassing effects during ELMs [8]. The outgassing may stem from D particles stored deeply in traps of the W-PFCs material (the amount of traps depends on the structure of the W-solute as well as the number of defects/traps produced by neutron irradiation). Also, D particle outgassing during an ELM has been observed also from Be-codeposited layers on the HFS upper baffle region in the JET-ILW [87]. To address the outgassing effect from metal surfaces and the impact on pedestal performance predictively the integrated code JINTRAC (a combination of the 1.5D core code JETTO with the EDGE2D-

EIRENE code) has been modified to include finite surface reservoirs in the PFCs [88]. In the model it was assumed that after emptying the surface reservoirs by an ELM heat pulse arriving at and heating up the PFC the recycling coefficient is reduced which in turns leads to a reduced fueling capacity after an ELM until the reservoirs are filled up again. As a principal result it was found that indeed a reduced recycling coefficient at the PFCs after an ELM crash leads to a delay in pedestal density increase and subsequently to lower confinement due to stiff core transport. However the pedestal model in JETTO was too simple as no direct coupling between density and temperature was included, hence there was no delay in pedestal temperature after the ELM. To improve this a coupling of particle and heat transport in the pedestal (e.g. [89]) in between ELMs should be implemented in JETTO. The retardation of the density built-up seen in the JINTRAC integrated model is also a strong function of the assumption of a varying recycling coefficient R between and at the ELM. To constrain the dynamic recycling better diffusive-trap models are being developed to derive time variation of R(t) which include the temperature variation of the material, varying trap densities in the solute as well as the variation of particle and heat flux prints during the ELM taking into account 2D effects a lateral transport effects within the material [9, 90]. With a more complete model for the evolution of fuel concentration in PFCs a better dynamic recycling can be developed to be linked with edge codes, going beyond the oversimplified surface reservoirs models used so far.

The previous example has highlighted what could be done with an integrated set of codes. However, progress in integrated (global) modelling is frustratingly slow as each individual sub-module has its own deficiencies which need to be resolved by separate validation activities. A full scenario modelling is still pending as important physics issues are still part of current research, to mention only a few: inter-ELM pedestal transport (beyond neo-classical approximations) and coupling of density and temperature transport, an ELM model which reflects the convective nature of filamentary transport, fueling models (in 2D/3D) for neutral penetration and pellet ablation models, kinetic corrections in parallel SOL transport (exploiting PIC simulations), robust anomalous transport models, full automatic coupling of PWI models coupled with edge codes, improvements of atomic & molecular physics models for volumetric and surface processes, etc. Furthermore it needs to be stressed that a pure technical coupling of physics modules does not necessarily mean elimination of unknowns (e.g. boundary conditions) of the prescribed global model as feedback mechanisms

between the sub-models increase the overall non-linearity of the numerical system making an achievement of total convergence hard.

8 Summary and conclusions

The absence of C in metallic devices does allow a disentanglement of relevant processes in the understanding of the power and particle exhaust problem. With metallic devices one can completely ignore the source and migration of eroded particles from amorphous C PFCs. Hydrocarbons created by the chemical erosion process which homogenize the plasma fueling process do not exist in metallic devices like AUG or JET-ILW. Instead the particle content is mainly driven by the particle throughput. Significant progress has been made in the validation of standard modelling tools like SOLPS or EDGE2D-EIRENE to predict reactor relevant conditions, i.e. dissipative radiative and detached divertors. Whereas somewhat robust scalings exist for the description of the upstream conditions (i.e. a scaling for the parallel heat flux density $q_{||}$, λ_q-scalings) a scaling for the dissipation in the divertor hardly exists as the parallel temperature drop towards the divertor plates is impacted by a manifold of physics effects: system size, divertor geometry, neutral compression, radiation loss, stiff 2D nature of transport in the SOL. However, with the numerical analysis of discharges in metallic devices some deficiencies in the understanding of the divertor physics and divertor operational conditions could be overcome and some of the most critical features which allow a robust and reliable predictions for dissipation in ITER or DEMO have been identified. Cross-field drifts play a major role as well as sophisticated neutral kinetic transport model which need to include important volumetric neutral processes (viscosity, molecular assisted processes, elastic and charge exchange processes). With metallic devices it has become clear that a full description of the vessel geometry that includes the sub-divertor region, leakages and gaps has become mandatory as otherwise neutral compression and conductance up to the pumps as well as plasma fueling cannot be adequately described. Oversimplified and reduced neutral models neglecting neutral ballistic effects are not necessarily rewarding in the understanding of the fueling process. Ultimately, a reliable and predictive edge model must reproduce the full cycle of the transition from an attached regime into the fully detached regime including the HFSHD region observed in various metallic devices. Some progress has been achieved in the understanding of the upstream pedestal pressure loss in case of significant impurity seeding. To achieve this, 2D edge models must extend the simulation grid into the pedestal region in order to rectify the impact of X-point radiation loss in the confined region. A suitable combination of transport in the pedestal as well as in the SOL not neglecting the

advective nature of anomalous transport is required. In view of integration of models taking into account also PWI as well as migration of intrinsic impurities like Be or W the edge models have been extended in order to allow for a plasma description up to the first-wall (e.g. SOLEDGE2D-EIRENE with a wide-grid option). With such upgraded tools plasma flows can be properly derived which in turn can be exploited by erosion codes like ERO or global migration codes like WallDYN. Such codes have been quite successful in reproducing ELM-induced W-sources, impurity flows into remote areas as well as global transport and flows of Be and deposition patterns. An important ingredient is a database reflecting details on the erosion mechanisms. Such databases are currently revised by using sophisticated molecular-dynamics codes. The progress in global scenario modelling using integrated codes like JINTRAC which couple self-consistently the various physics sub-systems with different transport time-scales (i.e. core / pedestal / edge / SOL / PFCs) is slow as each individual physics sub-model on its own requires careful validation. It is expected though that with the lack of C in metallic devices and with the inclusion of PWI models into integrated codes a more complete picture of the impact of the wall on plasma confinement can be drawn.

Acknowledgements

This work has been carried out within the framework of the EUROfusion Consortium and has received funding from the Euratom research and training programme 2014-2018 under grant agreement No 633053. The views and opinions expressed herein do not necessarily reflect those of the European Commission.

References

[1] R. Neu, et al., “Tungsten experiences in ASDEX Upgrade and JET”, Fusion Engineering (SOFE), IEEE 25th Symposium (2013) 1-8

[2] S. Brezinsek et al., Nucl. Fusion 53 (2013) 083023

[3] T. Loarer et al., J. Nucl. Mater. 463 (2015) 1117-1121

[4] M. Wischmeier et al., J. Nucl. Mater 463 (2015) 22-29

[5] R. Schneider et al., Contrib. Plasma Phys. 46, No. 1-2, 3 (2006) 191

[6] S. Brezinsek et al., Nucl. Fusion 55 (2015) 063021

[7] S. Brezinsek et al., J. Nucl. Mater 463 (2015) 11-21

[8] S. Brezinsek et al., Phys. Scr. (2016) 014076

[9] K Schmid Phys. Scr. (2016) 014025

[10] M. E. Fenstermacher et al., Plasma Phys. Contr. Fusion 41 (1999) A345-A355

[11] V. Kotov et al., Plasma Phys. Control. Fusion 50 (2008) 105012

[12] S. Wiesen et al., J. Nucl. Mater. 415 (2011) S535-S539

[13] C. Guillemaut et al., Nucl. Fusion 54 (2014) 093012

[14] S. Wiesen et al., J. Nuc. Mater. 463 (2015) 480-484

[15] R. Simonini et al., Contrib. Plasma Phys. 34 (1994) 368

[16] D. Reiter et al., J. Nucl. Mater. 196-198 (1992) 80

[17] S. Wiesen et al, ITC project report (2006), http://www.eirene.de/e2deir_report_30jun06.pdf

[18] H. Bufferand et al., J. Nuc. Mater. 438 (2013) S445-S448

[19] H. Kawashima, et al., Plasma Fusion Res. 1, (2006) 031

[20] K. Shimizu, et al., Nucl. Fusion 49 (2009) 065028

[21] T. Rognlien et al., J. Nucl. Mater., 196/198 (1992) 347

[22] P.C. Stangeby, “The Plasma Boundary of Magnetic Fusion Devices”, Institute of Physics Publishing, Bristol (2002)

[23] D. P. Stotler, C. F. F. Karney, Contrib. Plasma Phys. 34 (1994) 392

[24] H. Kawashima, K. Shimizu, T. Takizuka, et al., J. Nucl. Matter. 363-365 (2007) 786-790

[25] P.C. Stangeby Nucl. Fusion 52 (2012) 083012

[26] R.A. Pitts et al., J. Nucl. Mater. 313-316 (2003) 777

[27] M. Wischmeier et al., J. Nucl. Mater. 313-316 (2003) 980

[28] Feng Y., Sardei F., et al., J. Nucl. Mater. 313–316 (2003) 857

[29] Feng Y et al., Contrib. Plasma Phys. 54 (2014) 426

[30] O. Schmitz et al., Nucl. Fusion 56 (2016) 066008

[31] T. Eich et al., Nucl. Fusion 53 (2013) 093031

[32] B. Sieglin et al., Plasma Phys. Control. Fusion 55 (2013) 124039

[33] R.J. Goldston Nucl. Fusion 52 (2012) 013009

[34] E.T. Meier et al., this conference PSI 2016, P1.38

[35] T. Eich et al., Phys. Rev. Lett. 107 (2011) 215001

[36] A. Loarte et al., J. Nucl. Mater. 266-269 (1999) 587

[37] M. Makowski et al., Phys. Plasmas 19 (2012) 056122

[38] A. Scarabosio et al., J. Nucl. Mater. 463 (2015) 49

[39] M. Wischmeier, IAEA-FEC, St. Petersburg, Russia (2014)

[40] A. Kallenbach et al., Nucl. Fusion 55 (2015) 053026

[41] C. Giroud, IAEA-FEC, St. Petersburg, Russia (2014)

[42] A. Jarvinen et al., J. Nucl. Mater. 463 (2015) 135

[43] M. Reinke et al., this conference PSI 2016, I12

[44] A. Kallenbach et al., Plasma Phys. Control. Fusion 55 (2013) 124041

[45] S. Potzel et al., Nucl. Fusion 54 (2014) 013001

[46] F. Reimold et al., Nucl. Fusion 55 (2015) 033004

[47] F. Reimold et al., this conference PSI 2016, O15

[48] F. Reimold et al., J. Nucl. Mater. 463 (2015) 128

[49] S. Wiesen et al., J. Nucl. Mater. 415 (2011) S535-S539

[50] A. Jarvinen et al., “Impact of divertor geometry on radiative divertor performance in JET H-mode plasmas”, subm. to PPCF (2015)

[51] L. Aho-Mantila et al., J. Nucl. Mater. 463 (2015) 546

[52] A. Kallenbach et al., IAEA-FEC 2012

[53] M. Groth et al., J. Nucl. Mater. 463 (2015) 471

[54] D. Moulton et al., Proc. 42nd EPS Conference on Plasma Physics (2015)

[55] S. Varoutis et al., subm. to NF (2015)

[56] C. Gleason-Gonzales et al., Fus. Eng. Des. 89 (2014) 1042-1047

[57] S. Lisgo et al., J. Nucl. Mater. 337–339 (2005) 139

[58] A. Kukushkin et al., Fusion Eng. Des. 86 (2011) 2865

[59] K. Lawson et al., this conference PSI 2016

[60] W. Dekeyser et al., this conference PSI 2016

[61] D. Carralero et al., J. Nucl. Mater. 463 (2015) 123

[62] A. Wynn et al., this conference PSI 2016

[63] B. Lipschultz et al., Plasma Phys. Control. Fusion 47 (2005) 1559

[64] O.E. Garcia et al., Plasma Phys. Control. Fusion 49 (2007) B47

[65] O.E. Garcia et al., this conference PSI 2016

[66] W. Fundamenski et al., Nucl. Fusion 47 (2007) 417

[67] D. Reiser et al., Physics of Plasmas, 14 (8) (2007) 082314

[68] C. Guillemaut et al., Nucl. Fusion 54 (2014) 093012

[69] K. Krieger, priv. Comm.

[70] C. Bjorkas et al., J. Nucl. Mater. 439, 1–3 (2013) 174

[71] S. Brezinsek et al., Nucl. Fusion 54 (2014) 103001

[72] E. Safi et al., J. Nucl. Mater. 463 (2015) 805

[73] A. Kirschner et al., J. Nucl. Mater. 463 (2015) 116

[74] K. Schmid et al., J. Nucl. Mater. 415 (2011) 284

[75] K. Schmid et al., J. Nucl. Mater. 438 (2013) S484

[76] M Mayer et al., Phys. Scr. (2016) 014051

[77] G. Meisl et al., this conference PSI 2016

[78] R. Dux et al., this conference PSI 2016

[79] M. Romanelli et al., Plasma and Fusion Research, Volume 9 (2014) 3403023

[80] G. Falchetto et al., “The European Integrated Tokamak Modelling (ITM) Effort:

Achievements and First Physics Results” IAEA-FEC (2014)

[81] R. Zagorski et al., Contrib. Plasma Phys. 48 (2008) 179

[82] H. Shirai er al., Plasma Phys. Control. Fusion 42 (2000) 1193

[83] E. Wolfrum et al., this conference PSI 2016

[84] E. de la Luna et al., IAEA-FEC, St. Petersburg, Russia (2014)

[85] P. Tamain et al., J. Nuc. Mat. 463 (2015) 450

[86] D. Harting et al., J. Nuc. Mat. 463 (2015) 493

[87] E. de la Cal, S. Brezinsek, priv. Comm. (2016)

[88] S. Wiesen et al., "Effect of PFC Recycling Conditions on JET Pedestal Density", in print, Contrib. Plasma Phys (2016)

[89] B. Scott et al., Gyrokinetic Theory and Dyanmics of the Tokamak Edge, Proc. 15th Plasma Edge Theory Conference (PET), Nara, Japan (2015)

[90] D. Matveev et al., this conference PSI 2016

Figure captions

Figure 1: From JET-C to JET ILW: C (CIII/neCIII/ne) and O edge plasma content (OVI/neOVI/ne) during the divertor phase as function of discharge number (reproduced from [7]).

Figure 2: Radiative power function $L_z(T_e)$ for Be, N and Ne. solid line: coronal approximation, dots: non-coronal approximation (including transport from EDGE2D-EIRENE [42])

Figure 3: Divertor evolution during detachment measured by spectroscopy in AUG. Active Langmuir probes are shown in red. The divertor spectroscopy lines of sight are shown in grey. (a) Transition from attached to fluctuating state (label FS) to partially detached outer target is shown. (b) Transition from partially detached outer target to completely detached targets is shown. (reproduced from [46])

Figure 4: Schematic comparison of vertical (VT) and horizontal (HT) target configuration in JET-ILW and neutral recycling sources and ballistic trajectories. The outgassing of D particle on top of the HFS baffle occurs during an ELM and has been measured by fast cameras [87]

Figure 5: Schematic of integration of codes

Figure 1

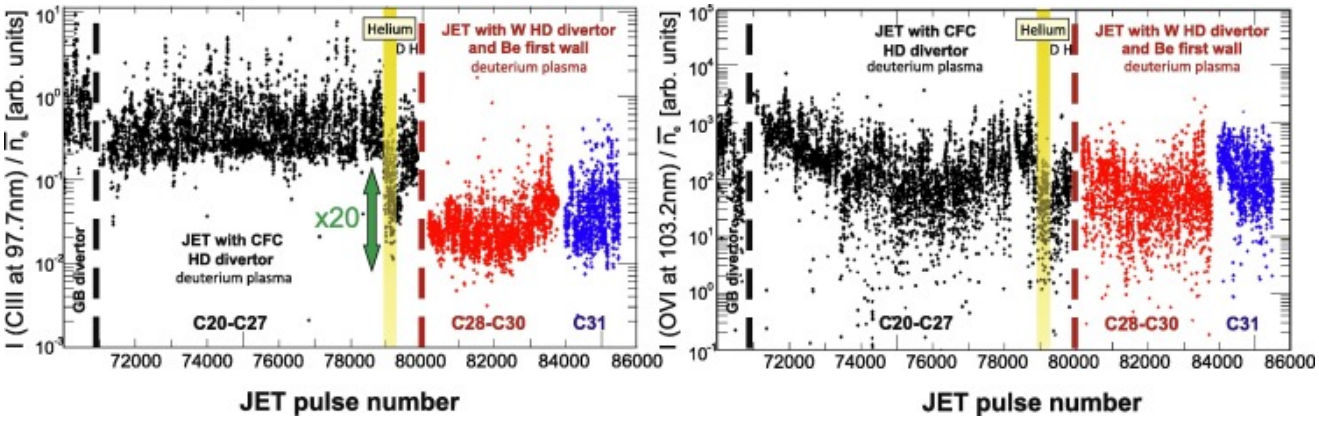
I (CIII at 97.7nm) / $\bar{n}_e$ [arb. units]
GB divertor
Helium
D H
JET with W HD divertor
and Be first wall
deuterium plasma
x20
JET with CFC
HD divertor
deuterium plasma
C20-C27
C28-C30
C31
72000 74000 76000 78000 80000 82000 84000 86000
JET pulse number
I (OVI at 103.2nm) / $\bar{n}_e$ [arb. units]
GB divertor
Helium
D H
JET with CFC
HD divertor
deuterium plasma
JET with W HD divertor
and Be first wall
deuterium plasma
C20-C27
C28-C30
C31
72000 74000 76000 78000 80000 82000 84000 86000
JET pulse number

Figure 2

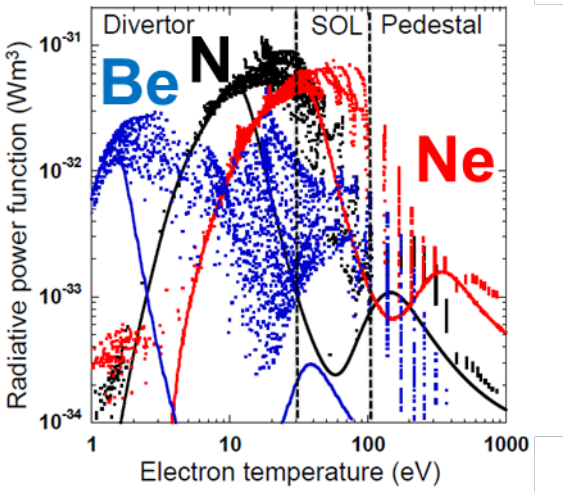
Divertor
SOL
Pedestal
Be
N
Ne
Radiative power function (Wm³)
10⁻³¹
10⁻³²
10⁻³³
10⁻³⁴
1
10
100
1000
Electron temperature (eV)

Figure 3

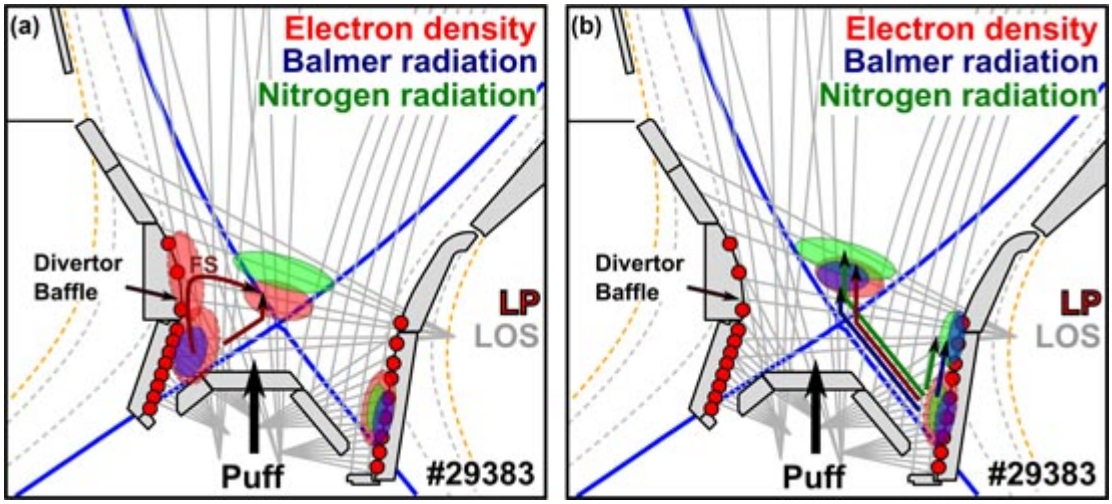
(a)
Electron density
Balmer radiation
Nitrogen radiation
Divertor
Baffle
FS
LP
LOS
Puff
#29383
(b)
Electron density
Balmer radiation
Nitrogen radiation
Divertor
Baffle
LP
LOS
Puff
#29383

Figure 4

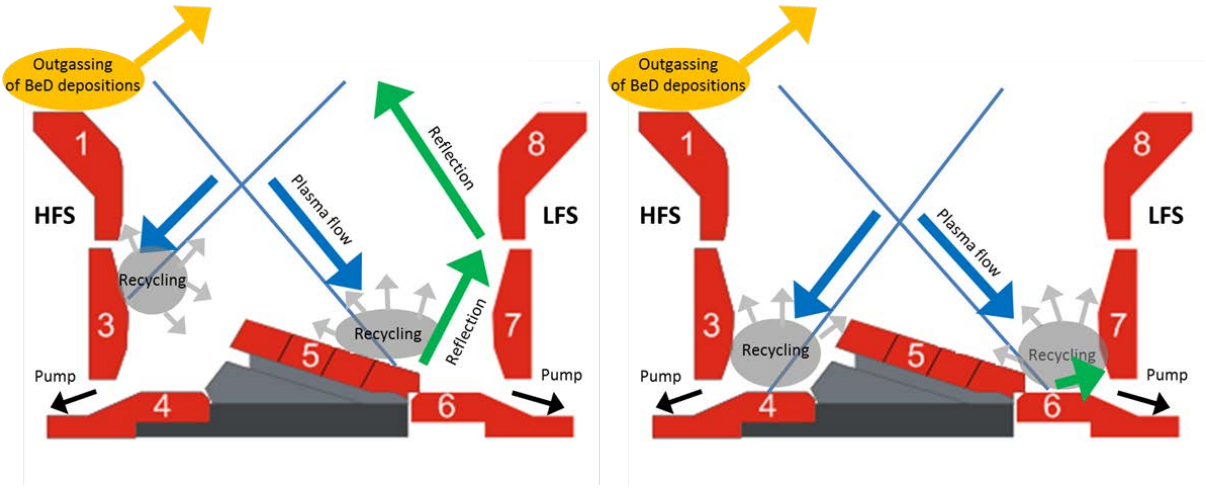
Outgassing
of BeD depositions
1
HFS
Recycling
3
Pump
4
Plasma flow
Reflection
Recycling
5
Reflection
8
LFS
7
Pump
6
Outgassing
of BeD depositions
1
HFS
3
Recycling
Pump
4
Plasma flow
5
Recycling
8
LFS
7
Pump
6

Figure 5

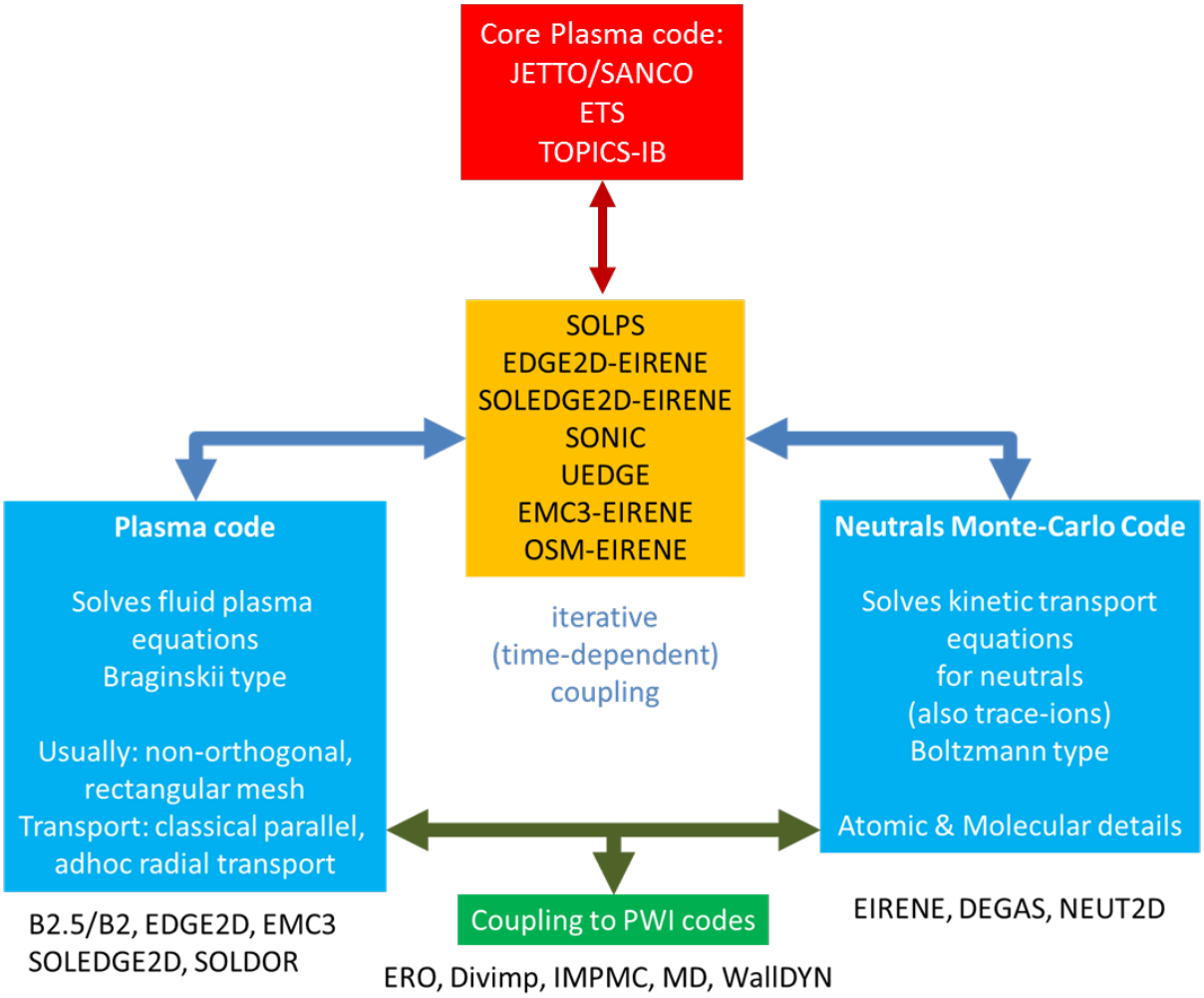
Core Plasma code:
JETTO/SANCO
ETS
TOPICS-IB
SOLPS
EDGE2D-EIRENE
SOLEDGE2D-EIRENE
SONIC
UEDGE
EMC3-EIRENE
OSM-EIRENE
iterative
(time-dependent)
coupling
Plasma code
Solves fluid plasma equations
Braginskii type
Usually: non-orthogonal, rectangular mesh
Transport: classical parallel, adhoc radial transport
B2.5/B2, EDGE2D, EMC3
SOLEDGE2D, SOLDOR
Neutrals Monte-Carlo Code
Solves kinetic transport equations
for neutrals
(also trace-ions)
Boltzmann type
Atomic & Molecular details
EIRENE, DEGAS, NEUT2D
Coupling to PWI codes
ERO, Divimp, IMPMC, MD, WallDYN